Melting heat transfer of a non-Newtonian phase change material in a cylindrical vertical-cavity partially filled porous media

Received 1 August 2019
Revised 1 October 2019
Accepted 15 October 2019

Mohammad Ghalambaz
Department for Management of Science and Technology Development, Ton Duc Thang University, Ho Chi Minh City, Vietnam and Faculty of Applied Sciences, Ton Duc Thang University, Ho Chi Minh City, Vietnam

Kasra Ayoubi Ayoubloo
Department of Mechanical Engineering, Faculty of Engineering, Shahid Chamran University of Ahvaz, Ahvaz, Iran, and

Ahmad Hajjar
LabECAM, ECAM Lyon, Université de Lyon, Lyon, France

Abstract

Purpose – This paper aims to investigate melting heat transfer of a non-Newtonian phase change material (PCM) in a cylindrical enclosure-space between two tubes using a deformed mesh method.

Design/methodology/approach – Metal foam porous layers support the inner and outer walls of the enclosure. The porous layers and clear space of the enclosure are filled with PCM. The natural convection effects during the phase change are taken into account, and the governing equations for the molten region and solid region of the enclosure are introduced. The governing equations are transformed into non-dimensional form and then solved using finite element method. The results are compared with the literary works and found in good agreement. The non-Newtonian effects on the phase change heat transfer and melting front are studied.

Findings – The results show that the increase of non-Newtonian effects (the decrease of the power-law index) enhances the heat melting process in the cavity at the moderate times of phase change heat transfer. The temperature gradients in porous metal foam over the hot wall are small, and hence, the porous layer notably increases the melting rate. When the melting front reaches the cold porous layer, strong non-linear behaviors of the melting front can be observed.

Originality/value – The phase change heat transfer of non-Newtonian fluid in a cylindrical enclosure partially filled with metal foams is addressed for the first time.

Keywords Non-Newtonian fluid, Cylindrical vertical-cavity, Melting phase change, Porous metal foam

Paper type Research paper

Nomenclature

L_f = latent heat of fusion *(J/kg)*;
u_r = radial velocity *(m/s)*;
u_z = vertical velocity *(m/s)*;
ΔT = temperature difference;

International Journal of Numerical Methods for Heat & Fluid Flow
Vol. 30 No. 7, 2020
pp. 3765-3789

0961-5539
DOI 10.1108/HFF-08-2019-0620

C = specific heat ($J/kg.K$);
C_p = specific heat in constant pressure ($J/kg.K$);
Da = Darcy number;
g = gravity (m/s^2);
$\dot{G}$ = shear rate variable;
k = thermal conductivity ($W/m.K$);
L = height (m);
L = length of each porous layer;
m = consistency index;
$M1$ *and* $M2$ = dummy variables;
n = non-Newtonian power-law index;
Nu = Nusselt number;
P = non-dimensional pressure;
p = pressure (Pa);
Pr = Prandtl number;
R = radius of the cylinder;
r,z = cylindrical coordinates;
Ra = Rayleigh number;
Ste = Stefan number;
T = emperature (K);
t = time (s);
T_0 = initial temperature (K); and
T_f = melting temperature (K).

Greek symbols

μ = dynamic Viscosity ($kg/m.s$);
α = thermal diffusivity (m^2/s);
γ = shear rate (1/s);
ε = porosity;
θ = non-dimensional temperature;
τ = non-dimensional time;
β = thermal expansion coefficient ($1/K$);
κ = permeability;
ρ = density (kg/m^3)V; and
ν = kinematic viscosity (m^2/s).

Subscripts

1 = thickness of the inner porous layer;
2 = thickness of the outer porous layer;
C = Cold;
Eff = Effective;
h = hot
i = inner porous layer;
i = interface position;
k = node number;
l = liquid phase;
o = outer porous layer;
p = porous layer; and
s = solid phase.

Superscript
* = non-dimensional; and
^ = weighting function.

1. Introduction

Flow and heat transfer in cavities with porous media are of essential importance in many industrial and engineering applications, such as energy storage, geothermal systems, heat exchangers, and crystallization process. In applications related to energy storage, phase change materials (PCM) have been used as an alternative to classical storage techniques like thermochemical reactions widely. This is mainly because of their small volume change and large latent heat, where a small amount of PCM can absorb and store a large amount of heat in a solid-to-liquid process or release the same energy when the phase change is in the opposite direction.

Natural convection flows have been investigated in different cavity configurations, such as cavities with one layer of porous medium (Astanina *et al.*, 2019), conjugate heat transfer with a layer of porous medium (Alsabery *et al.*, 2019a), multiple layers of porous media (Mehryan *et al.*, 2019; Miroshnichenko *et al.*, 2018), tilted porous cavities (Sheremet and Pop, 2018), wavy-walled cavities (Alsabery *et al.*, 2019c; Alsabery *et al.*, 2018) and cavities filled with porous fins (Asl *et al.*, 2019). Other studies considered the natural convection of nanofluids in cavities with porous media (Dogonchi *et al.*, 2019; Sivasankaran *et al.*, 2018; Pop *et al.*, 2016). There are also some studies that investigated the natural convection of single and two-phase nanofluids (Chamkha *et al.*, 2016; Chamkha *et al.*, 2017; Alsabery *et al.*, 2019b), and phase change heat transfer nano-encapsulated suspensions (Ghalambaz *et al.*, 2019a; Ghalambaz *et al.*, 2019b). These studies were undergone using Newtonian fluids as the heat transfer medium.

Similarly, natural convection of non-Newtonian fluids in channel cavities has been addressed for several geometries, such as square cavities (Pishkar *et al.*, 2019), trapezoidal cavities filled with porous medium(Alsabery *et al.*, 2017), L-shaped cavities (Jahanbakhshi *et al.*, 2018), the space between two plates (Biswal *et al.*, 2019; Mohebbi *et al.*, 2019) and the space between horizontal eccentric annulus (Harab *et al.*, 2019). The case of non-Newtonian nanofluids in porous cavities has been also considered (Kefayati, 2016; Hatami and Ganji, 2014).

Regarding the natural convection of PCM in cavities, the first works considered the configuration of two adiabatic walls on the top and bottom and two isothermal walls. Bertrand *et al.* (1999) summarized various numerical and experimental studies dealing with this type of configuration, and presented results that were used as benchmark solutions for later investigations with different models and methods (Vogel and Thess, 2019; Li *et al.*, 2017; Gao *et al.*, 2017; Singh and Bhargava, 2015). In addition, Dhaidan and Khodadadi (2015) summed up the influence of various cavity shapes, while the effect of the cavity inclination (Yang *et al.*, 2019; Zennouhi *et al.*, 2015) and the presence of a magnetic field (Bondareva and Sheremet, 2017; Ghalambaz *et al.*, 2017b) have been also considered.

Works dealing with cavities heated from the bottom, in which a Rayleigh-Benard flow could occur, have been relatively limited. However, these works gave more attention to the flow patterns inside the cavity. For instance, Gau and Viskanta (1983) observed experimentally the generation of inside flow regime for a substance with high Prandtl number melting in a cavity heated from the bottom. Gong and Mujumdar (1998) conducted a numerical study and found that increasing Ra leads to instability in natural convection. Recent studies focused on the enhancement of heat transfer in cavities heated from below using additives under different conditions (Mehryan *et al.*, 2018;

Sheikholeslami and Mahian, 2019; Ghalambaz *et al.*, 2017a; Motahar *et al.*, 2017). Additional works extended the study conditions and considered cavities heated from different sides and with different geometrical configurations (Dai *et al.*, 2018; Iachachene *et al.*, 2019; Ghosh *et al.*, 2019).

Cavities with porous media, mainly in the form of metal foam, also have been widely considered in heat transfer enhancement of PCM. In fact, it has been found analytically, numerically and experimentally that using metal foams increases substantially the thermal conductivity of PCM (Siahpush *et al.*, 2008; Tian and Zhao, 2013; Chen *et al.*, 2014; Xiao *et al.*, 2013; Xiao *et al.*, 2014). Zhao *et al.* (2010) concluded in their experimental analysis that the heat transfer enhancement of PCM depends on the material of the foam and its structure. Lafdi *et al.* (2007) used aluminum foam and found that conduction dominates the heat transfer when the foam porosity is low while convection becomes more effective when the porosity increases. This result was confirmed in the numerical study of Jourabian *et al.* (2018b) and Jourabian *et al.* (2018a), who considered the melting of ice and other PCM in annular cavities. Recently, Dinesh and Bhattacharya (2019) showed numerically that the duration of the energy absorption depends on the foam geometry, characterized by the porosity, the pore size, and the pore overlap. In their experimental-numerical analysis, Wu *et al.* (2018) compared the flow and heat transfer behaviors of Newtonian fluids, PCM, and composite PCM in a cavity, in which parallel steel wires are embedded, and thus, forming a two-dimensional porous structure. They concluded that increasing *Ra* lead to a stronger natural convection of the Newtonian fluid, while in the case of a PCM, decreasing the porosity weakened the natural convection and the heat transfer was dominated by conduction.

To sum up, the flow and heat transfer of Newtonian and non-Newtonian fluids, as well as of PCMs in cavities with or without porous media have been widely investigated. However, the rheological properties of the PCM have not been taken into account. As some PCM present a non-Newtonian fluid behavior (Wang *et al.*, 2019), the objective of the current study is to investigate the flow and heat transfer of non-Newtonian melting PCM in a cavity between two co-axial cylinders with porous media. Another aspect that this paper is trying to investigate is the presence of two layers of porous media with different metallic materials. The power-law model is used for the fluid. The study particularly aims to assess the effects of Rayleigh number, Darcy number and the power-law index on the melting liquid fraction and the variation of the melting interface. The paper is organized as follows: The geometrical and mathematical models are introduced in Section 2, and the equations governing heat transfer and fluid flow are formulated in the dimensionless form. In Section 3, the numerical method used to solve the non-dimensional equations is shown. The validation of the method by comparing its solutions to benchmark solutions is also illustrated. The results of the numerical study are then presented and thoroughly discussed in Section 4. Section 5 is a conclusion where the main results are summarized, and future work directions are discussed.

2. Geometric and mathematical models

2.1 Physics of the problem

A cylindrical enclosure with height L, inner radius of r_i and outer radius r_o, is filled with a PCM. Each of the inner and outer vertical walls of the enclosure is covered with a layer of porous metal foam. The thickness of the porous layers at the inner and outer walls are l_1 and l_2, respectively. The physical model of the enclosure and the coordinate system are depicted in Figure 1. The inner wall is isothermal at a hot temperature T_h while the outer wall is at a

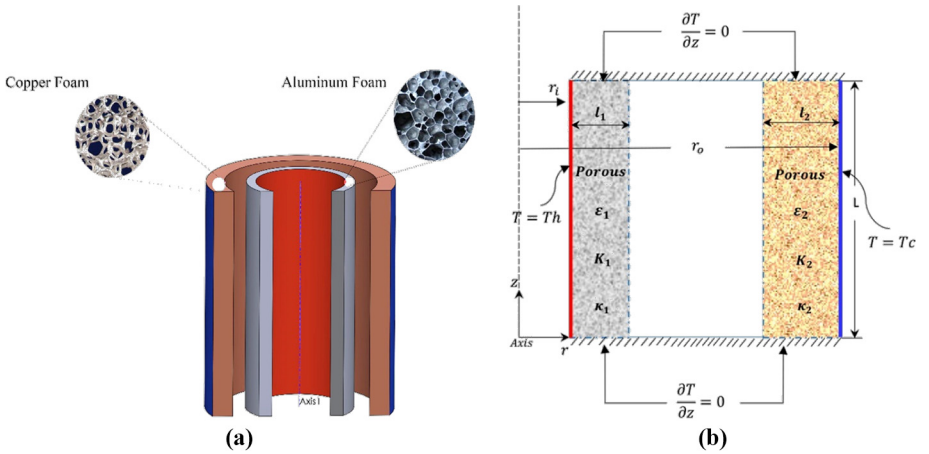

Notes: (a) 3D view of the model; (b) 2D view of the model

Figure 1. Schematic representation of the physical problem

cold temperature T_c. The top and bottom walls are well insulated. The porous layers for inner and outer walls are indicated by subscripts of 1 and 2, respectively. The porosity and the permeability of porous metal foams are denoted by ε and κ, respectively. The enclosure and the porous layers are completely filled with the PCM.

In this study, the enclosure is considered as axisymmetric, and the flow is unsteady, laminar and non-Newtonian. The radiation effects are assumed to be negligible, and the buoyancy forces are modeled using the Boussinesq approximation. The PCM is in the solid phase at a uniform temperature of T_c. The temperature of the inner wall suddenly raises to an isothermal temperature T_h and remains constant.

2.2 Governing equations

The continuity and momentum equations for a two-dimensional non-Newtonian fluid in a cylindrical coordinates system of (r, z), are as follows:

$$\rho \nabla^* . (\vec{u}) \tag{1}$$

where $\vec{u}$ is the vector of velocity.

$$\frac{\rho}{\varepsilon}\frac{\partial \vec{u}}{\partial t} + \frac{\rho}{\varepsilon^2}.(\vec{u}.\nabla^*)\vec{u} = \nabla^*.\left[-pI + \frac{\mu}{\varepsilon}\left(\nabla\vec{u} + (\nabla\vec{u})^T\right] - \frac{\mu}{\kappa}\vec{u} + \rho\vec{g}\beta\left(T - T_f\right)\right. \tag{2}$$

in which ρ, ε, t, p, μ, β, κ and $\vec{g}$ are, respectively, density, porosity, time, pressure, dynamic viscosity, volumetric thermal expansion coefficient, permeability and gravity, respectively. Here, the dynamic viscosity, μ, is not a constant and is a function of shear rate. To consider the non-Newtonian behavior of the fluid, the power-law is used. Based on this model dynamic viscosity can be written as (Shenoy, 2018):

$$\mu(\dot{\gamma}) = m\mu_a \rightarrow \begin{cases} \mu_a = (\dot{\gamma})^{n-1} \\ \dot{\gamma} = max\left(\sqrt{[D'] : [D']}, \dot{\gamma}_{\min}\right) \\ D' = \frac{1}{2}\left(\nabla\vec{u} + (\nabla\vec{u})^T\right) \end{cases} \tag{3}$$

where m is a consistency index for non-Newtonian viscosity, and n is called power-law index. Here $\dot{\gamma}$ is the shear rate. The deviation of n from unity indicates the degree of deviation from Newtonian behavior that is <1 for pseudoplastic, = 1 for Newtonian, and >1 for dilatant fluids. Pseudoplastic fluids are characterized by an apparent viscosity, which decreases with increasing shear rate; however, in dilatant fluids, the apparent viscosity increases with increasing shear rate.

Energy equation for melted PCM is expressed as follows:

$$(\rho c_p)_{eff,l}\frac{\partial T}{\partial t} + (\rho c_p)_l \vec{u}.\nabla^* T = \nabla^*.\left(k_{eff,l}\nabla^* T\right) \tag{4}$$

The energy equation for the solid PCM is as follows:

$$(\rho c_p)_{eff,s}\frac{\partial T}{\partial t} = \nabla^*.\left(k_{eff,s}\nabla^* T\right) \tag{5}$$

where in the above equations:

T is the temperature, C_p is the heat capacity at constant pressure, and k_{eff} is the effective thermal conductivity coefficient. The subscript "eff" denotes the effective properties of PCM and the porous layer. The superscript * in the above equations represents the dimensional variables. The effective heat capacity $(\rho C_p)_{eff}$ and the effective thermal conductivity k_{eff} in the above equations can be evaluated as (Nield and Bejan, 2013):

$$\begin{aligned} (\rho c)_{eff,l} &= (1-\varepsilon)(\rho c_p)_p + \varepsilon(\rho c_p)_l \\ k_{eff,l} &= (1-\varepsilon)k_p + \varepsilon k_l \end{aligned} \tag{6}$$

$$\begin{aligned} (\rho c)_{eff,s} &= (1-\varepsilon)(\rho c_p)_p + \varepsilon(\rho c_p)_s \\ k_{eff,s} &= (1-\varepsilon)k_p + \varepsilon k_s \end{aligned} \tag{7}$$

where ε is the porosity of each of the porous layers, and in the clear space with no porous layer, ε approaches to unity. In the present study, the volumetric changes due to phase change are neglected, and it is assumed that the density of the liquid is the same as density of the solid, and hence, as follows:

$$\rho_l = \rho_s = \rho \tag{8}$$

Considering the Stefan condition at the interface of phase change, the following energy balance equation can be considered for the displacement of the phase change interface:

$$k_{eff,l}\frac{\partial T}{\partial r}\bigg|_l - k_{eff,s}\frac{\partial T}{\partial r}\bigg|_s = \varepsilon\rho_l L_f u_r \tag{9}$$

$$k_{eff,l}\frac{\partial T}{\partial z}\bigg|_l - k_{eff,s}\frac{\partial T}{\partial z}\bigg|_s = \varepsilon \rho_l L_f u_z \tag{10}$$

According to the relations in equations (9) and (10), the equation for the velocity of the interface in r and z-directions are obtained as follows:

$$u_r = \frac{k_{eff,l}\frac{\partial T}{\partial r}\Big|_l - k_{eff,s}\frac{\partial T}{\partial r}\Big|_s}{\varepsilon \rho_l L_f} \tag{11}$$

$$u_z = \frac{k_{eff,l}\frac{\partial T}{\partial z}\Big|_l - k_{eff,s}\frac{\partial T}{\partial z}\Big|_s}{\varepsilon \rho_l L_f} \tag{12}$$

According to the model definition in Figure 1, the corresponding boundary conditions for equations (1), (2), (4) and (6) are:

$$r = r_i, z, t \to \vec{u} = 0, T = T_h \tag{13}$$

$$r = r_o, z, t \to \vec{u} = 0, T = T_c = T_f \tag{14}$$

$$r = r_f, z = z_f, \vec{u} = u_f, T = T_f \tag{15}$$

$$r, z = 0, t \to \vec{u} = 0, \frac{\partial T}{\partial z} = 0 \tag{16}$$

$$r, z = L, t \to \vec{u} = 0, \frac{\partial T}{\partial z} = 0 \tag{17}$$

The initial condition of the problem is also defined as the equation below:

$$r, z, t = 0 \to \vec{u} = 0, T = T_0 \tag{18}$$

The initial temperature is assumed equal to the cold temperature T_c, and hence, $T_0 = T_c = T_f$.

The dimensionless variables in these equations are defined as:

$$R = \frac{r}{L}, Z = \frac{z}{L}, \vec{U} = \frac{\vec{u}L}{\alpha_l}, \theta = \frac{T - T_f}{T_h - T_f}, \tau = \frac{t\alpha_l}{L^2}, P = \frac{pL^2}{\rho \alpha_l^2}, \alpha_l = \frac{k_l}{(\rho c_p)_l}, Pr = \frac{m}{\rho}\frac{\alpha_l^{n-2}}{L^{2n-2}},$$

$$Ra = \frac{\rho g \beta (T_h - T_f) L^{2n+1}}{m\alpha_l^n}, Da = \frac{\kappa}{L^2}, Ste = \frac{c_p(T_h - T_f)}{L_f}, k_{(s/l)} = \frac{k_s}{k_l}, \rho c_{(p/l)} = \frac{(\rho c_p)_P}{(\rho c_p)_l},$$

$$(\rho c_p)_{s/l} = \frac{(\rho c_p)_s}{(\rho c_p)_l}, k_{p/l} = \frac{k_p}{k_l}$$

$$L_1 = \frac{l_1}{L}, L_2 = \frac{l_2}{L} \tag{19}$$

where *Pr*, *Ra*, *Da* and *Ste* are the Prandtl number, Rayleigh number, Darcy number and Stefan number, respectively. Some of the non-dimensional parameters are adopted from Cao and Faghri (1990).

Introducing the above dimensionless dependent and independent variables in the governing equations, the following equations are obtained:

$$\rho\left(\nabla.\overrightarrow{U}\right) = 0 \tag{20}$$

$$\frac{1}{\varepsilon}\frac{\partial \overrightarrow{U}}{\partial t} + \frac{1}{\varepsilon^2}.\left(\overrightarrow{U}.\nabla\right)\overrightarrow{U} = \nabla.\left[-Pl + \frac{\mathrm{Pr}\dot{G}^{n-1}}{\varepsilon}\left(\nabla\overrightarrow{U} + \left(\nabla\overrightarrow{U}\right)^T\right] - \frac{\mathrm{Pr}}{Da}\dot{G}^{n-1}\overrightarrow{U} + PrRa\,\theta_z\right. \tag{21}$$

Energy conservation for melted PCM:

$$\left((1-\varepsilon)\frac{(\rho c_p)_p}{(\rho c_p)_l} + \varepsilon\right)\frac{\partial\theta}{\partial\tau} + \left(\overrightarrow{U}.\nabla\theta\right) = \left((1-\varepsilon)\frac{k_p}{k_l} + \varepsilon\right)\nabla^2\theta \tag{22}$$

Energy conservation for solid PCM:

$$\left((1-\varepsilon)\frac{(\rho c_p)_p}{(\rho c_p)_l} + \varepsilon\frac{(\rho c_p)_s}{(\rho c_p)_l}\right)\frac{\partial\theta}{\partial\tau} = \left((1-\varepsilon)\frac{k_p}{k_l} + \varepsilon\frac{k_s}{k_l}\right)\nabla^2\theta \tag{23}$$

The boundary conditions are also transformed into the following non-dimensional form:

$$R = R_i, Z, \tau \to \overrightarrow{U} = 0, \theta = 1 \tag{24}$$

$$R = R_o, Z, \tau \to \overrightarrow{U} = 0, \theta = 0 \tag{25}$$

$$R = R_f, Z = Z_f, \overrightarrow{U} = 0, \theta = 0 \tag{26}$$

$$R, Z = 0, \tau \to \overrightarrow{U} = 0, \frac{\partial\theta}{\partial Z} = 0 \tag{27}$$

$$R, Z = 1, \tau \to \overrightarrow{U} = 0, \frac{\partial\theta}{\partial Z} = 0 \tag{28}$$

$$R, Z, \tau = 0 \to \overrightarrow{U} = 0, \theta_0 = \frac{T_0 - T_f}{T_h - T_f} = 0 \tag{29}$$

Here, the parameters of interest are the volume fraction of melt and the Nusselt number at the hot wall. The volume fraction of melt is normalized with respect to the volume of the void space in the cavity. The void space in the porous space and the clear space is filled with PCM. Hence, the normalized melt volume fraction is introduced as:

$$NVF = \frac{\int_0^1 \int_{R_i}^{R_m} 2\pi r \varepsilon(R) dR dZ}{\int_0^1 \int_{R_i}^{R_o} 2\pi r \varepsilon(R) dR dZ} \tag{30}$$

where NVF denotes the Normalized Volume Fraction of the melt and the subscript m denotes the location of the melt-solid interface. As the cavity is cylindrical, the elements are axis-symmetric, thus, an element far away from the axis contains more volume compared to an element near the axis. Hence, the integrals of equation (30), sweep over the cylindrical space.

The heat transfer at the surface of the hot wall is defined using the energy balance at the surface as $h(T_h - T_c) = -k_{eff,l}(\partial T/\partial r)|_{r=ri}$. At the initial time, there is a very thin layer of molten PCM at the hot surface. Hence, the effective thermal conductivity of the liquid PCM and porous medium is adopted. Using the non-dimensional variables of equation (19), the local Nusselt number can be rewritten as:

$$Nu_Z = \frac{hZ}{k_{eff,l}} = \frac{\partial \theta}{\partial R}\Bigg)_{R=R_i} \tag{31}$$

where the average Nusselt number can be evaluated as:

$$Nu_{Avg.} = \int_o^1 Nu_Z dZ \tag{32}$$

3. Numerical method, grid check and validation

3.1 Numerical method

The finite element method is used to solve the governing equations. Following the standard finite element method, the governing equations are first written in a weak form and then integrated over the produced grid. The weak form of the equations can be written as:

$$-(1/\varepsilon) \times \text{test}(U) \times U_\tau + \text{test}(U_X) \times \left(-2 \times \left(\text{Pr}\,\dot{G}^{n-1}/\varepsilon\right) \times U_X + P\right) + \text{test}(U_Y) \times \left(-\left(\text{Pr}\dot{G}^{n-1}/\varepsilon\right) \times (U_Y + V_X)\right) + \text{test}(U)\,(\text{Pr/Da})\dot{G}^{n-1} \times U - (1/\varepsilon^2)\,\text{test}(U) \times (U \times U_X + V \times U_Y) + \text{Ra} \times \text{Pr} \times \text{test}(U) \times \theta \tag{33a}$$

$$-(1/\varepsilon) \times \text{test}(V) \times V_\tau + \text{test}(V_Y) \times \left(-2 \times \left(\text{Pr}\,\dot{G}^{n-1}/\varepsilon\right) \times V_Y + P\right) + \text{test}(V_X) \times \left(-\left(\text{Pr}\,\dot{G}^{n-1}/\varepsilon\right) \times (U_Y + V_X)\right) + \text{test}(V)\,(\text{Pr/Da})\dot{G}^{n-1} \times V - (1/\varepsilon^2)\,\text{test}(V) \times (U \times V_X + V \times V_Y) \tag{33b}$$

$$-\text{test}(P) \times (U_X + VY) \tag{33c}$$

$$-\text{M}_1 \times \text{test}(\theta) \times \theta_\tau - \text{test}(\theta) \times (U \times \theta_X + V \times \theta_Y) + \text{test}(\theta_X)\,\text{M}_2 \times (\theta_Y + \theta_X) \tag{33d}$$

where test(U), test(V), test(P) and test(θ), are the weighting function of $\hat{U}$, $\hat{V}$, $\hat{P}$ and $\hat{\theta}$, respectively. The subscript of τ denotes the time derivative while the subscripts of X and Y denote the spatial partial derivatives. In equation (33d), $\text{M}_1 = \left((1-\varepsilon)\frac{(\rho c_p)_p}{(\rho c_p)_l} + \varepsilon\right)$ and $\text{M}_2 = \left((1-\varepsilon)\frac{k_p}{k_l} + \varepsilon\right)$ in the melted region, and $\text{M}_1 = \left((1-\varepsilon)\frac{(\rho c_p)_p}{(\rho c_p)_l} + \varepsilon\frac{(\rho c_p)_s}{(\rho c_p)_l}\right)$ and $\text{M}_2 = \left((1-\varepsilon)\frac{k_p}{k_l} + \varepsilon\frac{k_s}{k_l}\right)$ in the solid region. Each of the above equations shall be integrated over the domain of the solution where here the integration sign is omitted for convenience.

Second-order Gaussian quadrature method was used for the integration of the residual equations. Then, the Newton method was used to iteratively solve the residual equations at each time step up to the relative accuracy of 10^{-3}. Adequate selection of time-step is very important in transient phase change problems, and hence, an automatic time-step scheme based on free-step automatic Backward Differentiation Formula (BDF) is used to handle the time-step sizes during the solution. The free-steps are controlled in the order of one and two using the BDF scheme (De Los Reyes and González Andrade, 2012). At each time step, the residual equations are interactively solved by using the Newton method based on a PARDISO solver (Schenk and Gärtner, 2004; Wriggers, 2008; Verbosio *et al.*, 2017) up to the absolute error of 10^{-6}. A fixed damping factor of 0.9 was adopted for the Newton method. Because of the limitation of our deformed grid approach in removing the deformed grids at the end of the phase change. The grid movement next to the cold wall was forced to zero to avoid the deformed grid collide with the cold wall. The grid-check and validations will be discussed in next sub-chapters.

3.2 Grid check

A grid independence test has been performed to find the acceptable grid size, with a reasonable computational cost and accuracy. To check the grid independency of the solution, the calculations were repeated for four types of triangular grids with sizes 1,993, 2,468, 2,717 and 3,316, and the computations are performed for the following set of non-dimensional parameters: $Pr = 60$, $Ra = 7 \times 10^5$, $Ste = 0.012$, $Da_1 = 1.2 \times 10^{-3}$, $Da_2 = 6 \times 10^{-3}$, $\varepsilon_{p1} = 0.2$, $\varepsilon_{p2} = 0.3$, $(\rho c_p)_s/(\rho c_p)_l = 1.15 \times 10^{-4}$, $(\rho c_p)_{p1}/(\rho c_p)_l = 1.6$, $(\rho c_p)_{p2}/(\rho c_p)_l = 2.3$, $k_s/k_l = 1$, $k_{p1}/k_l = 1000$, $k_{p2}/k_l = 2005$, $l_1 = 0.2$, $l_2 = 0.2$ and $n = 0.7$. These non-dimensional parameters are in agreement with Paraffin wax materials for PCM, and copper foam and aluminum foam for porous layers. In the present study, the thickness of the porous layers l_1 and l_2 is kept constant equal to 0.2.

The details of the used grids are reported in Table I.

The time history of the normal volume fraction of the melt is summarized in Table II for various grid sizes and time steps. The results of Table II indicate that the refining of the mesh shows a fluctuation but converging behavior. Grid of Case 3 provides about 4 per cent relative accuracy, which is acceptable for most engineering applications. Hence, Case 3 is adopted for computations. Moreover, the computational volume of the non-dimensional void space, which was used for the calculation of NVF was 4.002.

3.3 Validation

The results of the present model and numerical method are validated against several works available in the literature. As the first validation, the study of Basak *et al.* (2006) is adopted. Basak *et al.* (2006) addressed the free convection flow and heat transfer in a cavity filled with a porous medium. The vertical walls of the cavity were at isothermal cold temperature while the bottom of the cavity was as hot temperature. The top wall of the cavity was well insulated and considered as adiabatic. Figure 2 shows a comparison between the streamlines of the present study and those reported in Basak *et al.* (2006) when Ra = 10^6, Pr = 0.71 and Da = 10^{-5}. As seen, a very good agreement between the results of the present study and Basak *et al.* (2006).

Bertrand *et al.* (1999) investigated the phase change heat transfer in a cavity heated from the sidewall. A comparison between the results reported in Bertrand *et al.* (1999) and the results of the present study for a Newtonian fluid when $Pr = 50$, $n = 1$, $Ste = 0.1$ and $Ra =$

Cases	Grid size
Case 1	Consists of 1,993 domain elements and 163 boundary elements
Case 2	Consists of 2,107 domain elements and 185 boundary elements
Case 3	Consists of 2,486 domain elements and 223 boundary elements
Case 4	Consists of 3,316 domain elements and 275 boundary elements

Table I. Different grid-sizes for melting volume fraction

Cases	$\tau = 2$	$\tau = 3$	$\tau = 4$	*Max error (%)
Case 1	0.6426	0.8090	0.8363	10
Case 2	0.7482	0.8371	0.8521	4
Case 3	0.6884	0.8319	0.8521	4
Case 4	0.7183	0.8354	0.8521	–

Note: *Max Error = $|\text{NVF} - \text{NVF}_{@\text{Case4}}|/\text{NVF}_{@\text{Case4}}$

Table II. NVF at various time steps and grid sizes

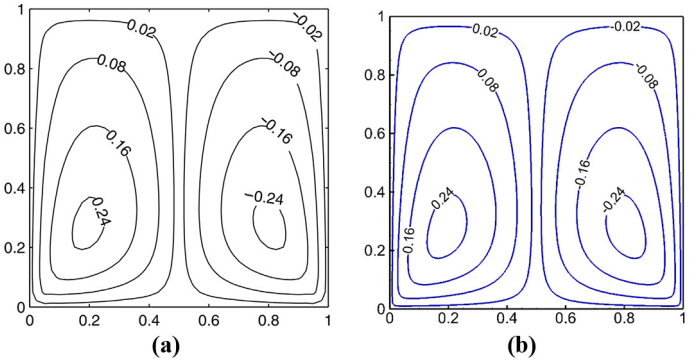

Source: (a) Basak *et al.* (2006); (b) present study

Figure 2. A comparison between the streamlines of the present study and the literature results when Ra = 10^6, Pr = 0.71 and Da = 10^{-5}

1×10^7 is performed and reported in Figure 3 at two different time steps of $Ste \times \tau = 0.002$ and 0.01. As seen, the trend of the results of the present study is in agreement with the literature data. However, there are also some differences between the outcomes of different researchers. The reason for such difference is that measuring an accurate melting interface in the experiment of Lacroix was difficult due to the fact that at the fusion state, the melting interface is soft. The divergence between the numerical results is because of the adopted models. The literature studied have used the enthalpy-porosity approach to model the phase change heat transfer. In the enthalpy-porosity approach, it is assumed that the phase change occurs at the fusion temperature range rather than a fixed fusion temperature. Thus, interpreting an accurate fusion interface depends on the size of the fusion temperature range. Using a narrow temperature range also results in discontinuity of heat equation, a problem, which researchers typically avoid by adopting a sufficiently wide fusion temperature range. Therefore, some differences between the results of literature studied could be expected.

Considering the heat transfer in porous media, the results are obtained for the natural convection in a trapezoidal porous cavity heated from below. The local Nusselt number is compared with the study of Basak *et al.* (2009) when $Da = 10^{-3}$, $Pr = 7.2$, $n = 1$ and $Ra = 10^6$. The results are plotted in Figure 4. This figure also depicts excellent agreement between the results.

Matin and Khan (2013) investigated the steady-state two-dimensional free convection of a power-law non-Newtonian fluid in a horizontal annulus enclosure. The inner and other walls of the enclosure are isothermal with temperature difference. A comparison between the average Nusselt number calculated in the present study and those reported by Matin and Khan (2013) is depicted in Figure 5 when $Ra = 10^3$ and $Pr = 10$ for various values of the non-Newtonian power-law index of n. As seen, there is an excellent agreement between the results.

As a final validation, the natural convection heat transfer in the space between two vertical annuli as addressed by Kakarantzas *et al.* (2017) is selected. In the absence of phase

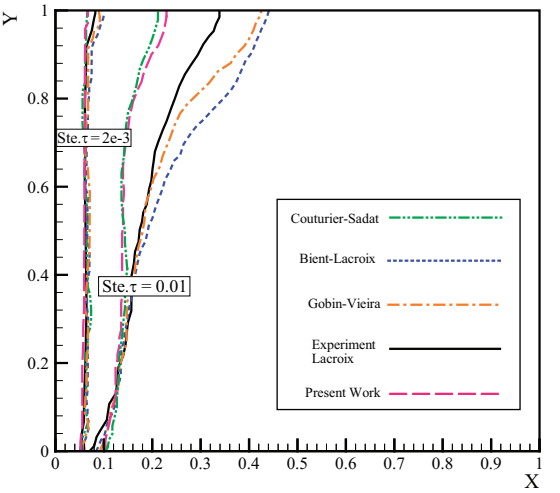

Source: Bertrand *et al.* (1999)

Figure 3.
A comparison between the results of the present study and the literature results

change or magnetic field effects, the temperature profile at the middle of hight of the enclosure along the radial direction is adopted for comparison. The results are plotted for a case with $Ra = 10^5$, $n = 1$ and $Pr = 0.0321$ in Figure 6 for two enclosure aspect ratios of $AR = 0.5$ and $AR = 1$. Figure 6 shows excellent agreement between the results.

4. Results and discussion

Using the above-described model, numerical computations were carried out to simulate the melting of a non-Newtonian PCM between two coaxial pipes, with the thickness of porous media being equal to $l_1 = 0.2$ and $l_2 = 0.2$ on the inner and outer pipes, respectively.

Figure 7 depicts the deformed grid patterns during the melting process for various Fourier number (τ). As depicted, the structured and unstructured grids are used to discretize melted fluid and solid substances, respectively. The used code uses a re-meshing technique during melting progress to improve the accuracy of the results. It is clear that the mesh is coarser in the solid region because of the fact that the temperature gradient in that region is

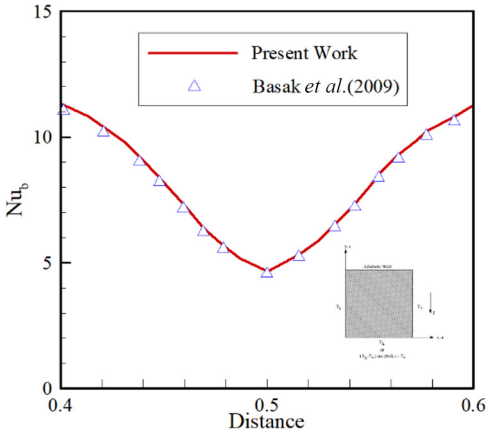

Figure 4.
Variation of local Nusselt number with distance for the bottom wall in the presence of uniform heating

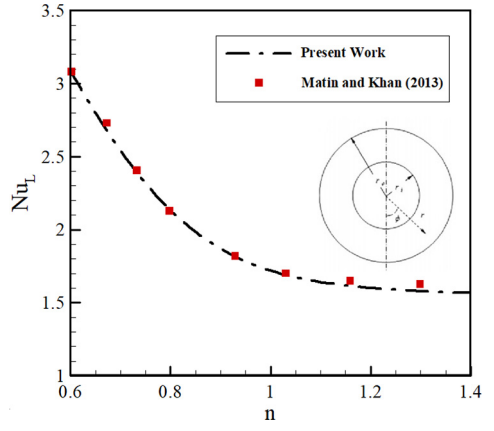

Figure 5.
A comparison between the results of present work and Matin and Khan (2013)

negligible. It is shown that increasing Fourier number leads to a larger melted liquid region and increases the depth of the melting front surface.

The effect of Fourier number τ on the streamlines and temperature contours during the melting process is illustrated in Figure 8. It can be seen that the streamlines, and consequently, the temperature contours, are noticeably influenced by τ. This is related to the change of the melted region, which is growing accordingly with τ. As this region grows, the streamlines are expanded throughout a greater area, and a circular shape can be seen in the center of the region. This also affects the temperature distribution, as the isotherms move closer to the cold wall.

Figure 9 illustrates the progress of the melt front for different values of τ. It shows that as τ increases, the depth of the melting front remarkably grows. The Fourier number is a dimensionless parameter, which represents the ratio between the conduction rate and the thermal energy storage rate during the time. In addition, it is shown that the melting regions increase drastically when τ is increased between 0.4 and 8. However, when τ is varied between 8 and 1000, the melting front is almost the same near the bottom wall, but it deflects toward the cold wall as it goes far from the bottom, thus, leading to an increase in the melting region surface.

The effect of Rayleigh number on the variation of the melting liquid fraction as a function of τ is illustrated in Figure 10, for $Da_1 = Da_2 = 1.2 \times 10^{-3}$, $\varepsilon_{p1} = \varepsilon_{p2} = 0.2$, $(\rho c_p)_{p1}/(\rho c_p)_l = (\rho c_p)_{p2}/(\rho c_p)_l = 1.6$ and $k_{p1}/k_l = k_{p2}/k_l = 1{,}000$. The remaining properties, such as Prandtl number, Stefan number, Darcy number, the thickness of the porous layers and non-Newtonian power-law index, are set equal to the default values. It can be seen that for low values of τ, mainly lower than 1, *Ra* has little effect on the variation of the liquid fraction. As *Ra* increases, a higher liquid fraction is obtained for the same value of τ, and consequently, complete melting is attained earlier.

The melting front for different Rayleigh numbers, at $\tau = 0.1$, $\tau = 1$, $\tau = 5$ and $\tau = 500$, is depicted in Figure 11. It is shown that for $\tau = 0.1$, the melting front remains almost the same when *Ra* increases. This is, as the heat transfer is a conduction-dominant regime at the early stage of the melting heat transfer. Moreover, the presence of the metal foam also weakens the convection heat transfer regime in the porous domain. Hence, the increase of the Rayleigh number does not induce a notable influence on the melting interface. For $\tau = 1$, increasing *Ra* moves the melting front toward the cold wall, and thus, leads to a larger meting region, especially in the center of the cavity and near the top wall. This behavior is less evident near the bottom wall. For $\tau = 100$, the melting region grows when *Ra* increases. The melting front is almost the same near the top wall and close to the cold wall, and its

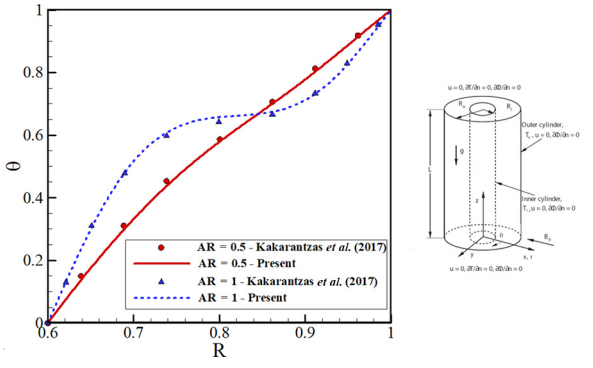

Figure 6.
A comparison between the temperature profile along the radial direction at the middle heights of the cavity addressed by Kakarantzas *et al.* (2017)

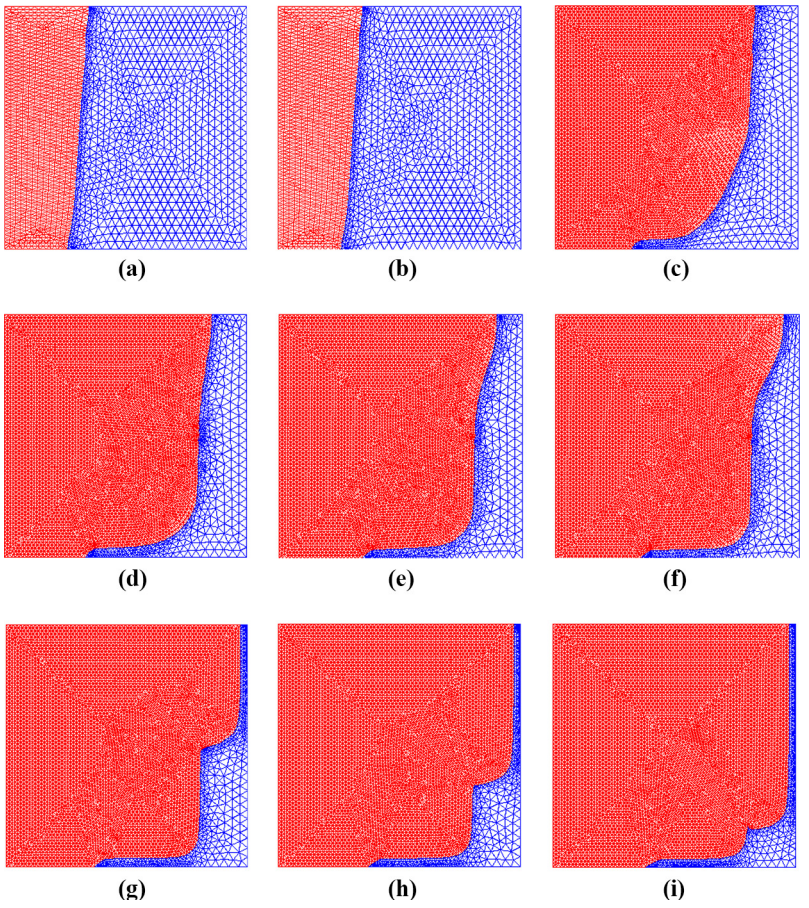

Figure 7. Display of the deformable mesh during melting process for (a) $\tau = 0.6$; (b) $\tau = 1.6$; (c) $\tau = 2.6$; (d) $\tau = 4.6$; (e) $\tau = 6.6$; (f) $\tau = 8.6$; (g) $\tau = 50$; (h) $\tau = 200$; and (i) $\tau = 1{,}000$

variation is occurring near the middle of the height. Similar behavior can be seen for $\tau = 500$. However, the variation of the melting region is less evident as the melting front is almost the same near the top and bottom walls, and is slightly deviating near the middle of the height.

The effects of the Darcy number *Da* on the melting liquid fraction and on the melting front for the constant parameters mentioned above and $Da_1 = Da_2 = Da$ $\varepsilon_{p1} = \varepsilon_{p2} = 0.2$, $(\rho c_p)_{p1}/(\rho c_p)_l = (\rho c_p)_{p2}/(\rho c_p)_l = 1.6$ and $k_{p1}/k_l = k_{p2}/k_l = 1000$ are depicted in Figures 12 and 13, respectively. Figure 12 shows that a higher value of *Da* increases the liquid melting fraction when the value of τ is fixed. By consequence, complete melting is achieved earlier when *Da* increases. It is also shown that when Da is less than 10^{-5}, the melting liquid fraction remains almost the same for every value of τ. This is because, for the very low values of Darcy number, the porous medium is almost impermeable, and there is a very weak natural convection flow in the metal foam layer. Hence, a further decrease of Darcy number does not influence the thermal behavior of the cavity, as the natural convection flow is suppressed in the porous layer.

In Figure 13, it can be seen that varying *Da* has little effect on the melting interface for $\tau = 0.1$ (Figure 13(a)), $\tau = 1$ (Figure 13(b)) and $\tau = 500$ (Figure 13(d)). Conversely, for

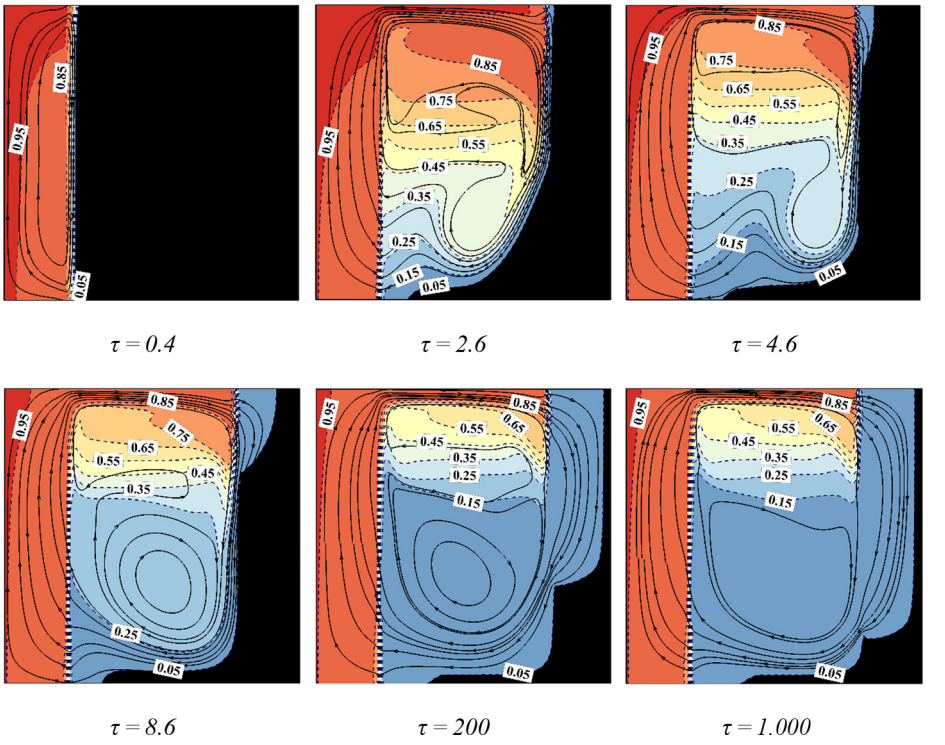

Figure 8.
Display of streamlines and isotherms during phase change at various non-dimensional time steps (τ)

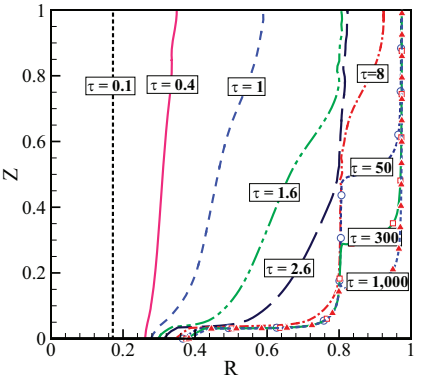

Figure 9.
The progress of the melting front during the melting process

$\tau = 5$ (Figure 13(c)), increasing *Da* moves the melting interface toward the cold wall and increases the size of the melting region. As mentioned, in the early stages of the melting process, the heat transfer mechanism is conduction dominant. Hence, as the flow circulation is weak the effect of Darcy number is not notable. At the middle of the melting process, the natural convection flows in the clear region of the cavity, which is in the molten state gets stronger. At this stage, any convection flow inside the porous

layer gets important as it interacts with the high thermally conductive metal foam and gets notably hot. Thus, as seen in Figure 13(c), the effect of Darcy number at the middle of the melting process is notable on the advancement of the melting interface. Moreover, the effect of Darcy number gets weaken at the end of melting process as the interface enter the metal foam layer again and the natural convection-dominant heat transfer shifts to the conduction-dominant heat transfer. Besides, the melting front and the size of the melting region are the same in all the cases when Da is lower than 10^{-5}.

Figure 14 illustrates the effect of the non-Newtonian index n on the melting liquid fraction for different values of τ. It shows that decreasing n, and thus, increasing the non-Newtonian effects in the liquid, increases the liquid fraction for the same value of τ. This also indicates an earlier complete melting for a higher value of n. Moreover, it can be seen that n has almost no effect when $\tau < 0.5$. This is, as the melting interface is in the porous layer with a conduction-dominant heat transfer mechanism at the early stage of phase change. Hence, the flow circulation, and thereby, the n effects are very weak.

Figure 15 depicts the effect of n on the melt interface and the size of the melting region. It is shown that while decreasing n for $\tau = 0.1$moves the melt front toward the hot wall and reduces the size of the melting region, increasing n for $\tau = 1$ leads to an opposite result and grows the melting region. For $\tau = 5$, the melting interface does not change substantially when n is varied between 0.7 and 0.9. When $n = 0.5$, the melting interface moves closer to the cold wall near the top of the cavity and farther toward the hot wall near the bottom, and the overall size of the melting region is slightly reduced. For $\tau = 500$, the melting interface is the same near the top and toward the middle for all the values of n, and deviates near the bottom wall. Therefore, the general result is that the effect of n on the melting interface is greatly affected by τ, and no general trend of variation can be inferred.

5. Conclusion

The phase change heat transfer of a non-Newtonian PCM in a cylindrical enclosure partially filled with two layers of the porous medium was theoretically addressed. A deformed grid approach is used to model the phase change heat transfer at an exact fusion temperature. The governing equations are transformed into a non-dimensional form and then solved using the finite element method. Grid study was performed, and the results were compared with various works available in the literature and found in good agreement. The effects of Darcy number, Rayleigh number and the non-Newtonian power-law index on the phase

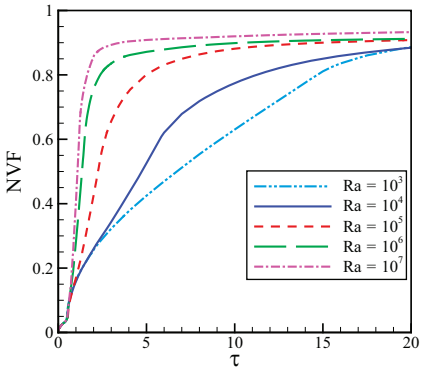

Figure 10.
The effect of Rayleigh numbers on the melting liquid fraction

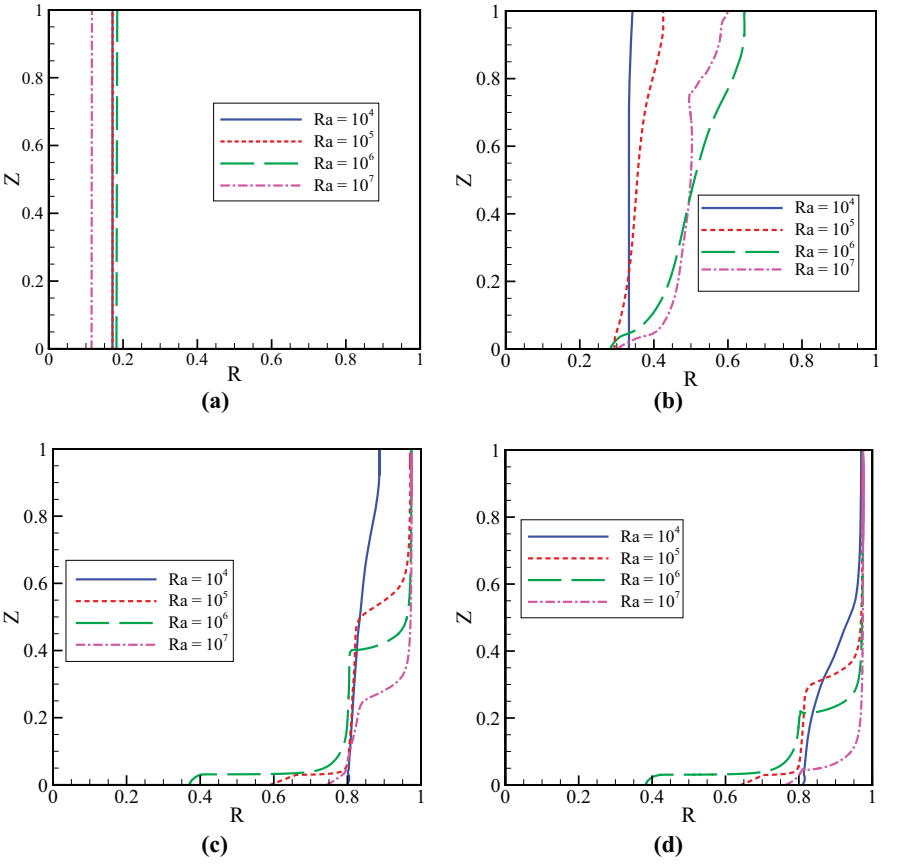

Figure 11.
The results for the interface melt for different Rayleigh numbers at (a) τ = 0.1; (b) τ = 1; (c) τ = 5; and (d) τ = 500

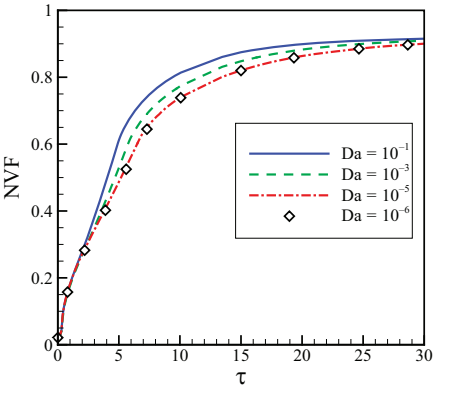

Figure 12.
The effect of Darcy numbers on the melting liquid fraction

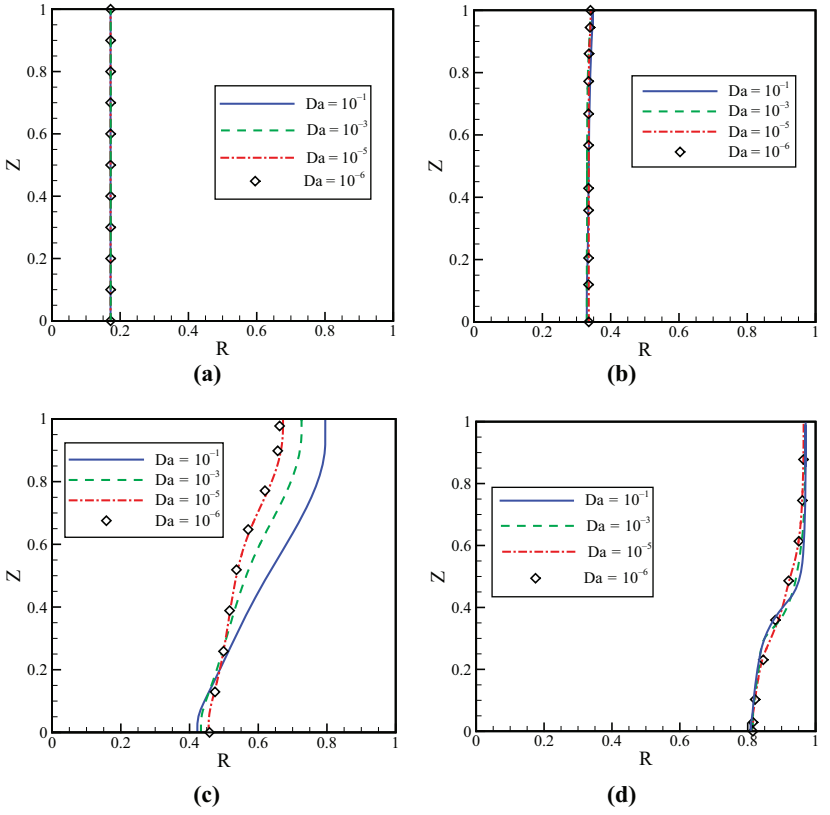

Figure 13.
The results for the interface melt for different Darcy numbers at (a) τ = 0.1; (b) τ = 1; (c) τ = 5; and (d) τ = 500

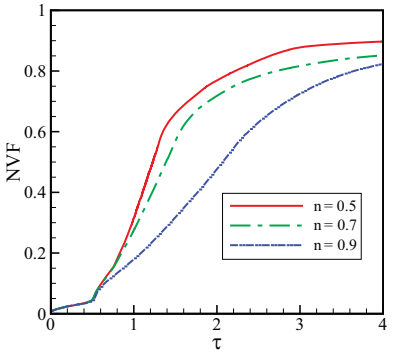

Figure 14.
The effect of the non-Newtonian power-law index (n) on the melting liquid fraction

change heat transfer and melt volume fraction were investigated in the enclosure. The main outcomes of the present study can be summarized as below:

- the results of the deformed grid approach are in good agreement with the results available in the literature. Hence, the deformed grid approach can model the phase

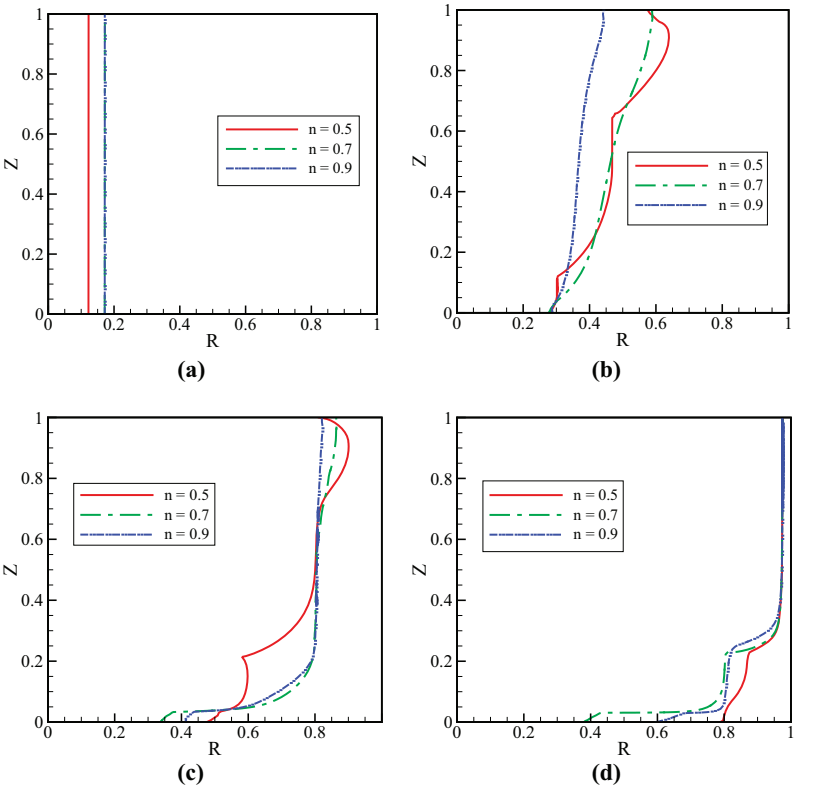

Figure 15.
The results for the interface melt for different non-Newtonian index at (a) $\tau = 0.1$; (b) $\tau = 1$; (c) $\tau = 5$; and (d) $\tau = 500$

change heat transfer in models involving natural convection effects using Stephan condition at an exact fusion temperature;

- in the porous layer, over the hot surface, the transfer is a conduction dominant heat transfer mechanism with a very low-temperature gradient. Hence, the porous layer over the hot wall mainly acts as an isotherm layer containing PCM;
- the increase of Rayleigh number up to order of 10^5 significantly accelerates the melting process as it changes the conduction heat transfer dominant regime to a convection-dominant regime. Further increase of Rayleigh number slightly enhances the melting process. In the case of Rayleigh number higher 10^5, the patterns of natural convection start to shift from top to bottom area of the enclosure;
- the increase of Darcy number enhances the melting process by allowing flow circulation in the porous layers. However, this effect is only important when the Darcy number is sufficiently large as an order of 0.1. Considering small values of Darcy number (order of 10^{-5}) the porous layer does not allow flow in the layer and further variation of Darcy number does not change the heat transfer behavior of the enclosure; and
- the decrease of the non-Newtonian power-law index (n) significantly enhances the melting process, particularly at middle stages of the phase change heat transfer. At

large times, when the flow reaches the cold porous layer, some non-linear behavior for the melting front and phase change heat transfer can be observed. Indeed, the increase of non-Newtonian effects (decrease of n) also notably affects the shape of melting front at large times.

The results of the present study indicate that the power-law index significantly affects the melting heat transfer in the enclosure. Moreover, the temperature gradients at the hot porous layer were small, while there was a significant temperature gradient at the clear region of the enclosure with no porous media. Hence, it can be concluded that the used metal foam enhanced the thermal conductivity in the porous layer. Maybe, using a porous metal foam with higher porosity but with a wider layer or a non-uniform porous layer results in more enhancement of heat transfer and phase change with a similar metal foam mass. Therefore, optimization of the porous layer for each index of the non-Newtonian power-law can be subject of future studies.

References

Alsabery, A., Chamkha, A., Saleh, H. and Hashim, I. (2017), "Transient natural convective heat transfer in a trapezoidal cavity filled with non-Newtonian nanofluid with sinusoidal boundary conditions on both sidewalls", *Powder Technology*, Vol. 308, pp. 214-234.

Alsabery, A., Yazdi, M., Altawallbeh, A. and Hashim, I. (2019a), "Effects of nonhomogeneous nanofluid model on convective heat transfer in partially heated square cavity with conducting solid block", *Journal of Thermal Analysis and Calorimetry*, Vol. 136 No. 4, pp. 1489-1514.

Alsabery, A.I., Gedik, E., Chamkha, A.J. and Hashim, I. (2019b), "Impacts of heated rotating inner cylinder and two-phase nanofluid model on entropy generation and mixed convection in a square cavity", *Heat and Mass Transfer*, pp. 1-18, available at: https://doi.org/10.1007/s00231-019-02698-8

Alsabery, A.I., Mohebbi, R., Chamkha, A.J. and Hashim, I. (2019c), "Effect of local thermal non-equilibrium model on natural convection in a nanofluid-filled wavy-walled porous cavity containing inner solid cylinder", *Chemical Engineering Science*, Vol. 201, pp. 247-263.

Alsabery, A.I., Tayebi, T., Chamkha, A.J. and Hashim, I. (2018), "Effect of rotating solid cylinder on entropy generation and convective heat transfer in a wavy porous cavity heated from below", *International Communications in Heat and Mass Transfer*, Vol. 95, pp. 197-209.

Asl, A.K., Hossainpour, S., Rashidi, M., Sheremet, M. and Yang, Z. (2019), "Comprehensive investigation of solid and porous fins influence on natural convection in an inclined rectangular enclosure", *International Journal of Heat and Mass Transfer*, Vol. 133, pp. 729-744.

Astanina, M.S., Sheremet, M. and Umavathi, C.J. (2019), "Unsteady natural convection in a partially porous cavity having a heat-generating source using local thermal non-equilibrium model", *International Journal of Numerical Methods for Heat and Fluid Flow*, Vol. 29 No. 6, pp. 1902-1919.

Basak, T., Roy, S., Paul, T. and Pop, I. (2006), "Natural convection in a square cavity filled with a porous medium: effects of various thermal boundary conditions", *International Journal of Heat and Mass Transfer*, Vol. 49 Nos 7/8, pp. 1430-1441.

Basak, T., Roy, S., Singh, A. and Balakrishnan, A. (2009), "Natural convection flows in porous trapezoidal enclosures with various inclination angles", *International Journal of Heat and Mass Transfer*, Vol. 52 Nos 19/20, pp. 4612-4623.

Bertrand, O., Binet, B., Combeau, H., Couturier, S., Delannoy, Y., Gobin, D., Lacroix, M., Le Quéré, P., Médale, M. and Mencinger, J. (1999), "Melting driven by natural convection a comparison exercise: first results", *International Journal of Thermal Sciences*, Vol. 38 No. 1, pp. 5-26.

Biswal, U., Chakraverty, S. and Ojha, B.K. (2019), "Natural convection of non-Newtonian nanofluid flow between two vertical parallel plates", *International Journal of Numerical Methods for Heat and Fluid Flow*, Vol. 29 No. 6, pp. 1984-2008.

Bondareva, N.S. and Sheremet, M.A. (2017), "Natural convection heat transfer combined with melting process in a cubical cavity under the effects of uniform inclined magnetic field and local heat source", *International Journal of Heat and Mass Transfer*, Vol. 108, pp. 1057-1067.

Cao, Y. and Faghri, A. (1990), "A numerical analysis of phase-change problems including natural convection", *Journal of Heat Transfer*, Vol. 12 No. 13, p. 112.

Chamkha, A., Doostanidezfuli, A., Izadpanahi, E. and Ghalambaz, M. (2017), "Phase-change heat transfer of single/hybrid nanoparticles-enhanced phase-change materials over a heated horizontal cylinder confined in a square cavity", *Advanced Powder Technology*, Vol. 28 No. 2, pp. 385-397.

Chamkha, A., Ismael, M., Kasaeipoor, A. and Armaghani, T. (2016), "Entropy generation and natural convection of CuO-water nanofluid in C-shaped cavity under magnetic field", *Entropy*, Vol. 18 No. 2, p. 50.

Chen, Z., Gao, D. and Shi, J. (2014), "Experimental and numerical study on melting of phase change materials in metal foams at pore scale", *International Journal of Heat and Mass Transfer*, Vol. 72, pp. 646-655.

Dai, R., Bian, Q., Wang, Q. and Zeng, M. (2018), "Evolution of natural convection melting inside cavity heated from different sides using enthalpy based lattice Boltzmann method", *International Journal of Heat and Mass Transfer*, Vol. 121, pp. 715-725.

De Los Reyes, J.C. and González Andrade, S. (2012), "A combined BDF-semismooth Newton approach for time-dependent Bingham flow", *Numerical Methods for Partial Differential Equations*, Vol. 28 No. 3, pp. 834-860.

Dhaidan, N.S. and Khodadadi, J. (2015), "Melting and convection of phase change materials in different shape containers: a review", *Renewable and Sustainable Energy Reviews*, Vol. 43, pp. 449-477.

Dinesh, B.V.S. and Bhattacharya, A. (2019), "Effect of foam geometry on heat absorption characteristics of PCM-metal foam composite thermal energy storage systems", *International Journal of Heat and Mass Transfer*, Vol. 134, pp. 866-883.

Dogonchi, A., Sheremet, M., Ganji, D. and Pop, I. (2019), "Free convection of copper–water nanofluid in a porous gap between hot rectangular cylinder and cold circular cylinder under the effect of inclined magnetic field", *Journal of Thermal Analysis and Calorimetry*, Vol. 135 No. 2, pp. 1171-1184.

Gao, D., Tian, F.-B., Chen, Z. and Zhang, D. (2017), "An improved lattice Boltzmann method for solid-liquid phase change in porous media under local thermal non-equilibrium conditions", *International Journal of Heat and Mass Transfer*, Vol. 110, pp. 58-62.

Gau, C. and Viskanta, R. (1983), "Flow visualization during solid-liquid phase change heat transfer I. Freezing in a rectangular cavity", *International Communications in Heat and Mass Transfer*, Vol. 10 No. 3, pp. 173-181.

Ghalambaz, M., Chamkha, A.J. and Wen, D. (2019a), "Natural convective flow and heat transfer of nano-encapsulated phase change materials (NEPCMs) in a cavity", *International Journal of Heat and Mass Transfer*, Vol. 138, pp. 738-749.

Ghalambaz, M., Groşan, T. and Pop, I. (2019b), "Mixed convection boundary layer flow and heat transfer over a vertical plate embedded in a porous medium filled with a suspension of nano-encapsulated phase change materials", *Journal of Molecular Liquids*, Vol. 293, pp. 111432.

Ghalambaz, M., Doostani, A., Izadpanahi, E. and Chamkha, A. (2017a), "Phase-change heat transfer in a cavity heated from below: the effect of utilizing single or hybrid nanoparticles as additives", *Journal of the Taiwan Institute of Chemical Engineers*, Vol. 72, pp. 104-115.

Ghalambaz, M., Doostanidezfuli, A., Zargartalebi, H. and Chamkha, A.J. (2017b), "MHD phase change heat transfer in an inclined enclosure: Effect of a magnetic field and cavity inclination", *Numerical Heat Transfer, Part A: Applications*, Vol. 71 No. 1, pp. 91-109.

Ghosh, D., Guha, C. and Ghose, J. (2019), "Numerical investigation of paraffin wax solidification in spherical and rectangular cavity", *Heat and Mass Transfer*, pp. 1-13, available at: https://doi.org/10.1007/s00231-019-02680-4

Gong, Z.X. and Mujumdar, A.S. (1998), "Flow and heat transfer in convection-dominated melting in a rectangular cavity heated from below", *International Journal of Heat and Mass Transfer*, Vol. 41 No. 17, pp. 2573-2580.

Harab, B.A., Calisir, T. and Baskaya, S. (2019), "Numerical investigation of transient natural convection heat transfer of non-Newtonian nanofluids between eccentric annulus", *Arabian Journal for Science and Engineering*, Vol. 44 No. 6, pp. 5631-5646.

Hatami, M. and Ganji, D. (2014), "Natural convection of sodium alginate (SA) non-Newtonian nanofluid flow between two vertical flat plates by analytical and numerical methods", *Case Studies in Thermal Engineering*, Vol. 2, pp. 14-22.

Iachachene, F., Haddad, Z., Oztop, H.F. and Abu-Nada, E. (2019), "Melting of phase change materials in a trapezoidal cavity: Orientation and nanoparticles effects", *Journal of Molecular Liquids*, Vol. 292, p. 110592, available at: https://doi.org/10.1016/j.molliq.2019.03.051

Jahanbakhshi, A., Nadooshan, A.A. and Bayareh, M. (2018), "Magnetic field effects on natural convection flow of a non-Newtonian fluid in an L-shaped enclosure", *Journal of Thermal Analysis and Calorimetry*, Vol. 133 No. 3, pp. 1407-1416.

Jourabian, M., Farhadi, M. and Darzi, A.R. (2018b), "Constrained ice melting around one cylinder in horizontal cavity accelerated using three heat transfer enhancement techniques", *International Journal of Thermal Sciences*, Vol. 125, pp. 231-247.

Jourabian, M., Darzi, A.A.R., Toghraie, D. and Ali Akbari, O. (2018a), "Melting process in porous media around two hot cylinders: Numerical study using the lattice Boltzmann method", *Physica A: Statistical Mechanics and Its Applications*, Vol. 509, pp. 316-335.

Kakarantzas, S., Benos, L.T., Sarris, I., Knaepen, B., Grecos, A. and Vlachos, N. (2017), "MHD liquid metal flow and heat transfer between vertical coaxial cylinders under horizontal magnetic field", *International Journal of Heat and Fluid Flow*, Vol. 65, pp. 342-351.

Kefayati, G. (2016), "Heat transfer and entropy generation of natural convection on non-Newtonian nanofluids in a porous cavity", *Powder Technology*, Vol. 299, pp. 127-149.

Lafdi, K., Mesalhy, O. and Shaikh, S. (2007), "Experimental study on the influence of foam porosity and pore size on the melting of phase change materials", *Journal of Applied Physics*, Vol. 102 No. 8, pp. 083549.

Li, D., Ren, Q., Tong, Z.-X. and He, Y.-L. (2017), "Lattice Boltzmann models for axisymmetric solid–liquid phase change", *International Journal of Heat and Mass Transfer*, Vol. 112, pp. 795-804.

Matin, M.H. and Khan, W.A. (2013), "Laminar natural convection of non-Newtonian power-law fluids between concentric circular cylinders", *International Communications in Heat and Mass Transfer*, Vol. 43, pp. 112-121.

Mehryan, S., Izadi, M., Chamkha, A.J. and Sheremet, M.A. (2018), "Natural convection and entropy generation of a ferrofluid in a square enclosure under the effect of a horizontal periodic magnetic field", *Journal of Molecular Liquids*, Vol. 263, pp. 510-525.

Mehryan, S., Sheremet, M.A., Soltani, M. and Izadi, M. (2019), "Natural convection of magnetic hybrid nanofluid inside a double-porous medium using two-equation energy model", *Journal of Molecular Liquids*, Vol. 277, pp. 959-970.

Miroshnichenko, I.V., Sheremet, M.A., Oztop, H.F. and Abu-Hamdeh, N. (2018), "Natural convection of alumina-water nanofluid in an open cavity having multiple porous layers", *International Journal of Heat and Mass Transfer*, Vol. 125, pp. 648-657.

Mohebbi, R., Delouei, A.A., Jamali, A., Izadi, M. and Mohamad, A.A. (2019), "Pore-scale simulation of non-Newtonian power-law fluid flow and forced convection in partially porous media: thermal lattice Boltzmann method", *Physica A: Statistical Mechanics and Its Applications*, Vol. 525, pp. 642-656.

Motahar, S., Alemrajabi, A.A. and Khodabandeh, R. (2017), "Experimental investigation on heat transfer characteristics during melting of a phase change material with dispersed TiO2 nanoparticles in a rectangular enclosure", *International Journal of Heat and Mass Transfer*, Vol. 109, pp. 134-146.

Nield, D.A. and Bejan, A. (2013), *Convection in Porous Media*, Springer, New York, NY, Heidelberg Dordrecht.

Pishkar, I., Ghasemi, B., Raisi, A. and Aminossadati, S.M. (2019), "Numerical study of unsteady natural convection heat transfer of Newtonian and non-Newtonian fluids in a square enclosure under oscillating heat flux", *Journal of Thermal Analysis and Calorimetry*, Vol. 138 No. 2, pp. 1697-1710.

Pop, I., Ghalambaz, M. and Sheremet, M. (2016), "Free convection in a square porous cavity filled with a nanofluid using thermal non equilibrium and Buongiorno models", *International Journal of Numerical Methods for Heat and Fluid Flow*, Vol. 26, pp. 671-693.

Schenk, O. and Gärtner, K. (2004), "Solving unsymmetric sparse systems of linear equations with PARDISO", *Future Generation Computer Systems*, Vol. 20 No. 3, pp. 475-487.

Sheikholeslami, M. and Mahian, O. (2019), "Enhancement of PCM solidification using inorganic nanoparticles and an external magnetic field with application in energy storage systems", *Journal of Cleaner Production*, Vol. 215, pp. 963-977.

Shenoy, A. (2018), *Heat Transfer to Non-Newtonian Fluids: Fundamentals and Analytical Expressions*, John Wiley and Sons.

Sheremet, M.A. and Pop, I. (2018), "Effect of local heater size and position on natural convection in a tilted nanofluid porous cavity using LTNE and Buongiorno's models", *Journal of Molecular Liquids*, Vol. 266, pp. 19-28.

Siahpush, A., O'Brien, J. and Crepeau, J. (2008), "Phase change heat transfer enhancement using copper porous foam", *Journal of Heat Transfer*, Vol. 130 No. 8, p. 082301.

Singh, S. and Bhargava, R. (2015), "Numerical simulation of a phase transition problem with natural convection using hybrid FEM/EFGM technique", *International Journal of Numerical Methods for Heat and Fluid Flow*, Vol. 25, pp. 570-592.

Sivasankaran, S., Alsabery, A. and Hashim, I. (2018), "Internal heat generation effect on transient natural convection in a nanofluid-saturated local thermal non-equilibrium porous inclined cavity", *Physica A: Statistical Mechanics and Its Applications*, Vol. 509, pp. 275-293.

Tian, Y. and Zhao, C. (2013), "Thermal and exergetic analysis of metal foam-enhanced cascaded thermal energy storage (MF-CTES)", *International Journal of Heat and Mass Transfer*, Vol. 58 Nos 1/2, pp. 86-96.

Verbosio, F., DE Coninck, A., Kourounis, D. and Schenk, O. (2017), "Enhancing the scalability of selected inversion factorization algorithms in genomic prediction", *Journal of Computational Science*, Vol. 22, pp. 99-108.

Vogel, J. and Thess, A. (2019), "Validation of a numerical model with a benchmark experiment for melting governed by natural convection in latent thermal energy storage", *Applied Thermal Engineering*, Vol. 148, pp. 147-159.

Wang, F., Lin, W., Ling, Z. and Fang, X. (2019), "A comprehensive review on phase change material emulsions: fabrication, characteristics, and heat transfer performance", *Solar Energy Materials and Solar Cells*, Vol. 191, pp. 218-234.

Wriggers, P. (2008), *Nonlinear Finite Element Methods*, Springer Science and Business Media.

Wu, Z.G., Sheng, W.C., Tao, W.Q. and Li, Z. (2018), "A novel experimental-numerical method for studying the thermal behaviors of phase change material in a porous cavity", *Solar Energy*, Vol. 169, pp. 325-334.

Xiao, X., Zhang, P. and Li, M. (2013), "Preparation and thermal characterization of paraffin/metal foam composite phase change material", *Applied Energy*, Vol. 112, pp. 1357-1366.

Xiao, X., Zhang, P. and Li, M. (2014), "Effective thermal conductivity of open-cell metal foams impregnated with pure paraffin for latent heat storage", *International Journal of Thermal Sciences*, Vol. 81, pp. 94-105.

Yang, X., Guo, Z., Liu, Y., Jin, L. and He, Y.-L. (2019), "Effect of inclination on the thermal response of composite phase change materials for thermal energy storage", *Applied Energy*, Vol. 238, pp. 22-33.

Zennouhi, H., Benomar, W., EL Rhafiki, T., Arid, A., Msaad, A.A. and Kousksou, T. (2015), "Numerical simulation of phase change material melting in inclined enclosure", *2015 3rd International Renewable and Sustainable Energy Conference (IRSEC)*, *IEEE*, p. 1-6.

Zhao, C., Lu, W. and Tian, Y. (2010), "Heat transfer enhancement for thermal energy storage using metal foams embedded within phase change materials (PCMs)", *Solar Energy*, Vol. 84 No. 8, pp. 1402-1412.

Corresponding author
Mohammad Ghalambaz can be contacted at: mohammad.ghalambaz@tdtu.edu.vn